ASF Alaska Satellite Facility News & Notes
Spring 2007, volume 4:1

Fine Beam RADARSAT-1 for Monitoring Pond Dynamics in the Alaskan Boreal Forest

By Dave Verbyla, Department of Forest Sciences, University of Alaska Fairbanks

Several recent scientific studies have used historic remotely-sensed imagery to document a substantial reduction in the number and size of ponds in many boreal regions of Alaska, including interior Alaska, the Kenai Peninsula, and the Seward Peninsula. This reduction may be associated with climate warming effects such as increased transpiration and evaporation of water during longer above-freezing seasons. In regions of discontinuous permafrost, shrinking ponds may also be due to thinning permafrost and development of unfrozen zones beneath ponds, called taliks, allowing for drainage.

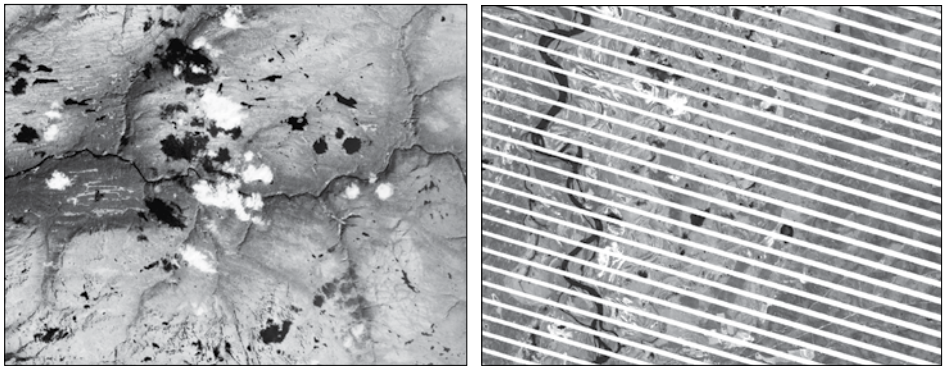

Figure 1. Landsat images from areas within Denali National Park, Alaska. a) Short-wave infrared TM image with less than 10 percent cloud cover. Notice that cloud shadows to the northwest of each cloud are dark and appear similar to ponds that are also in the image. b) ETM+ image near the edge of a scene with data gaps due to failure of the scan line corrector. Up to 25 percent of the image can be unusable due to the SLC problem.

Shallow lakes and ponds are of particular concern because they are important habitat for a variety of mammals and waterfowl, and they are the most susceptible to drying in a warming climate. By monitoring the dynamics of open water from spring break-up to fall freeze-up, it is possible to classify boreal ponds as deep and stable ponds versus shallow and ephemeral ponds likely to succeed to terrestrial habitat under a warmer climate.

One potential source of imagery for monitoring lakes and ponds across boreal Alaska is Landsat Thematic Mapper (TM) and Enhanced Thematic Mapper (ETM+) imagery, available on an 8-day orbit. There are two problems with this source of imagery. First, since TM and ETM+ are optical sensors, cloud cover limits the ability to delineate ponds, especially at high latitudes where cloud shadows cover a greater area than the clouds. For example a scene with 25 percent cloud cover could be over 60 percent unusable due to clouds and cloud shadow. Shadows are especially problematic when trying to spectrally classify ponds using optical data, as open water and shadow both have low spectral reflectance in most reflective bands. Second, the Scan Line Corrector (SLC) failed in Landsat-7 ETM+, creating gaps in images, especially away from the center of an image (Figure 1).

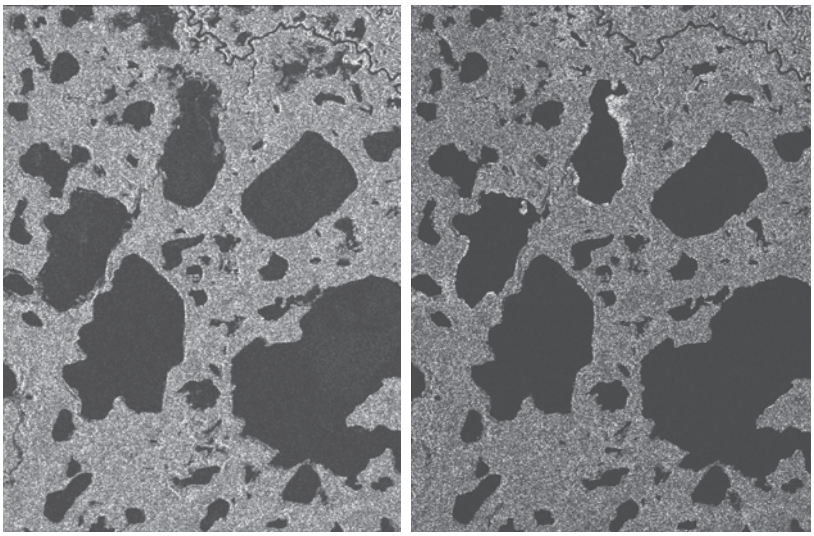

Figure 2. a) RADARSAT-1 fine beam image 21-May-2005. b) RADARSAT-1 fine beam image 14-June-2005.

One potential alternative to optical imagery for monitoring interseasonal pond dynamics is Synthetic Aperture Radar (SAR) imagery. Since many of the shallow ponds in boreal Alaska are relatively small, I requested RADARSAT-1 fine-beam mode acquired on at least a 2-week interval during the unfrozen period of April to October 2005 as a test case for the Michumina Basin in Denali National Park. RADARSAT-1 data were downloaded via ftp and processed to geotiff images using the ASF Convert tool. The Convert tool was used to resample the imagery to an Alaska Albers projection with a 6-m pixel size. The resulting images were then spatially co-registered using a linear rectification model based on locations that were visible on at least two images. Once a time series of RADARSAT-1 images were spatially co-registered (Figure 2), ponds that changed could be visualized by displaying a SAR image from two time periods as a red-green-blue color composite, where areas that changed from water to land would appear green on the color composite.

Continued on Page 2

Continued from front page

It is possible to create polygons representing ponds and lakes from any RADARSAT-1 image by using some Geographic Information Systems (GIS) techniques. I used an unsupervised classification technique to group pixels with similar values into classes. One problem inherent with this approach is that some isolated pixels are typically misclassified due to the speckle nature of SAR data. These scattered pixels were eliminated by using a majority filter and then groups of connected water pixels were extracted using a GIS. These groups were then converted into polygons using a GIS.

One of the advantages of polygons is that metrics such as pond area and shoreline length can easily be computed for each water body using a GIS (Figure 3). Polygons can then easily be selected based on area criteria, for example, select and display all ponds greater than 1 hectare in area. Since this methodology can be applied to a time series of SAR images, ponds can be selected based on changes in area such as selection of all ponds that have decreased by at least 10 percent between two time periods or shorelines that have declined by at least 50 m.

For the 2005 season, the shallow lake surfaces peaked around May 20, following the spring snowmelt period. There was a slight decrease in surface area in all lakes throughout the summer until late September. Less than 5 percent of the lakes had a decrease in surface area, but the lakes that changed did so substantially (Figure 4). This seasonal pattern of lake surface water dynamics may differ considerably from year to year. For example, in 2003, the month of July had record precipitation, while in 2004, May was relatively wet, followed by a record drought period.

SAR is the only cost-effective way to monitor seasonal surface water dynamics across the remote Alaskan boreal landscape.

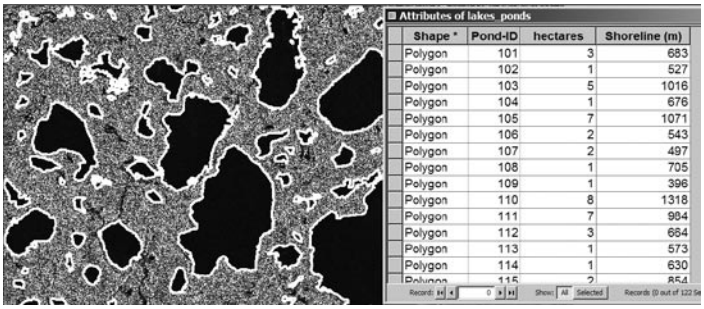

Shape *	Pond-ID	hectares	Shoreline (m)
Polygon	101	3	683
Polygon	102	1	527
Polygon	103	5	1016
Polygon	104	1	676
Polygon	105	7	1071
Polygon	106	2	543
Polygon	107	2	497
Polygon	108	1	705
Polygon	109	1	396
Polygon	110	8	1318
Polygon	111	7	984
Polygon	112	3	664
Polygon	113	1	573
Polygon	114	1	630

Figure 3. GIS polygons of lakes and ponds derived from RADARSAT-1 image. Since polygons are derived from a time series of RADARSAT-1 images, changes in surface water area or shoreline locations can easily be computed using a GIS.

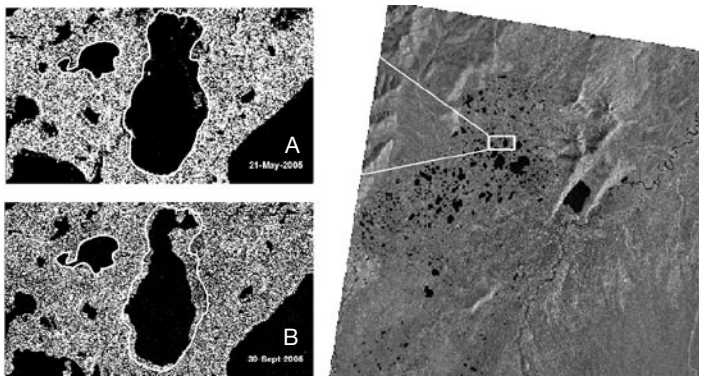

Figure 4. The small lake had little change in surface area between A and B, while the large lake decreased in area by 25%.

Uncertainties in Firn-Line Monitoring in Winter SAR Data

By Ian A. Brown
Department of Physical Geography and Quaternary Geology, Stockholm University, Sweden

Since the launch of ERS-1 in 1991, SAR imagery has become widely used in glaciology. The ability to image a surface, regardless of cloud cover and solar illumination, is particularly useful in a discipline which is often concerned with polar regions or areas with a prevalence of cloud cover. Sea ice monitoring in North America and northern Europe has been one of the great success stories of spaceborne SAR. Now operational glacier monitoring using optical-thermal and SAR systems are underway. For example, the Global Monitoring for Environment and Security (GMES) Polarview service provides products describing the position of facies boundaries at periodic intervals to support in situ mass-balance and runoff observations. The improvement in resolution and increased flexibility in imaging, inherent in the next generation systems, may lead to greater adoption of SAR in glacier monitoring.

One key parameter used in operational monitoring and glaciological research is the firn limit; the lower boundary of firn accumulation. Firn is snow left over from previous seasons that has been compacted and recrystallized. The firn limit equates to the equilibrium line: the boundary at which accumulation and ablation are equal and the glacier is in balance. On a valley, this boundary is generally assumed to conform laterally to the topography and can, therefore, be described by an altitude; the equilibrium line altitude (ELA). On an icecap, ELAs may be determined for different outlet glaciers or aspects to allow for differences in accumulation and ablation patterns. The ELA is frequently used to describe the annual 'state' of a glacier and is a common forcing mechanism in glacier-climate modelling.

In SAR images with dry snow conditions, the firn limit, a steady-state proxy of the ELA, can be identified as the lower limit of the bright scattering zone associated with firnification and percolation. This boundary may shift up-glacier as a result of increased melting on an annual basis. However, as firnification can take several years, increased accumulation may not be immediately identifiable in annual SAR images (as dry snow generates low volume scattering). The firn limit in SAR images is, therefore, marked by a degree of uncertainty unless there is a known net mass loss. Futhermore, the sensitivity of a SAR to firn thickness is not entirely understood. In optical images, snow a few centimeters thick may have the same signature as snow tens of metres thick covering 2 kilometers of glacier ice. In SAR data, dry snow, a few centimeters thick, may be undetectable and at what depth of firn the firn-limit threshold is reached may depend on the imaging geometry, snow/firn density and grain-size distribution. While firn-limit mapping is useful, further investigation is needed to refine the method.

Since 1998 we have collected RADARSAT-1 data on Blåmannsisen, an ice cap in north Norway. In 1998 and 2005, ground penetrating radar profiles (GPR) were taken in situ and an ASTER image from August 30th, 2001 was also acquired. The GPR profile from 1998 traversed the glacier from south to north. In the centre of the glacier, at an altitude of 1160 m, well above the firn limit, the GPR data indicated zones in which the snow and firn layering appear to have been planed off (removed by surface melting). The ASTER data from late summer 2001 also showed patches in which the annual snow cover had melted away exposing firn or ice. These zones, along with other zones of higher surface melt extracted from the ASTER image provide the opportunity to test whether the SAR data are sensitive to small changes in firn thickness. Additionally, by measuring backscatter near the firn limit relative to backscatter above and below the limit, we can refine our zonation of backscatter and ultimately may be able to determine the gradient in backscatter related to the gradient of firn depth from the firn limit up-glacier.

Six images were used in the analysis of backscatter signatures (Table 1). The images were calibrated and georeferenced using the ASF convert tool. The georeferencing was refined using a Rational Functions approach with a 30-m Digital Elevation Model (DEM) and 1:50000 scanned maps as the reference layers. The ASTER image was georeferenced using the Geomatica implementation of the Toutin method (satellite orbital modelling) with the same reference data. The SAR images were gereferenced to approximately 2 pixels (25-m) although the ASTER image appeared to have an offset of perhaps 5 pixels. It was not possible to determine whether there was a georeferencing bias in the middle of the icecap, so it was assumed that errors were more or less evenly distributed where surface slopes were low to moderate. From the ASTER data, a set of polygons was delimited describing different surface zones. Reference zones of firn and bare glacier ice were selected along with small patches of melt determined from ASTER and GPR data and other melt zones from the ASTER data alone. Given the small size of the melt patches observed in the ASTER and GPR data speckle filtering was not performed so as to limit the smoothing and resampling of the SAR data. A further class of "thin-firn" near the firn limit was delimited from the ASTER reference data.

Table 1. Image information and mean backscatter (dB) from reference polygons of different regions of the icecap (N, C, S, E and W refer to North, Central, South, East and West).

Image (Julian Day)	*Beam*	*Mean σ° Firn N*	*Mean σ° Firn C*	*Mean σ° Firn S*	*Mean σ° Ice N*	*Mean σ° Ice E*	*Mean σ° Ice W*
2000-31	ST3	-5.84	-6.11	-5.41	-3.08	-12.45	-13.53
2000-50	ST2	-2.32	-2.55	-3.17	-10.91	-9.92	-8.02
2000-98	ST2	-3.06	-3.16	-3.56	-10.52	-9.49	-7.83
2000-129	ST1	-3.16	-3.08	-3.90	-9.76	-8.68	-10.94
2000-304	ST1	-5.91	-5.67	-5.69	-4.72	-5.65	-2.96
2002-53	ST1	-2.13	-1.20	-3.47	-5.21	-4.52	-2.66
Mean		*-3.74*	*-3.63*	*-4.2*	*-7.37*	*-8.45*	*-7.66*

The polygons in the central icecap were digitized from the ASTER image and from the region identified in the GPR data. The polygons were small; in all, 11 polygons contained 466 pixels. The mean backscatter from these polygons was -3.56 dB, statistically inseparable from the firn classes. Larger polygons exhibiting melt derived from ASTER data alone had lower backscatter (mean -6.47 dB). The polygons adjacent to the firn limit, assumed to be containing thin firn, had mean backscatter values of -5.11 dB, -5.07 dB and -3.87 dB for northern, eastern, and western samples respectively (Figure 2). The original small patches could not be distinguished from the background signal of the firn area.

Continued on back page

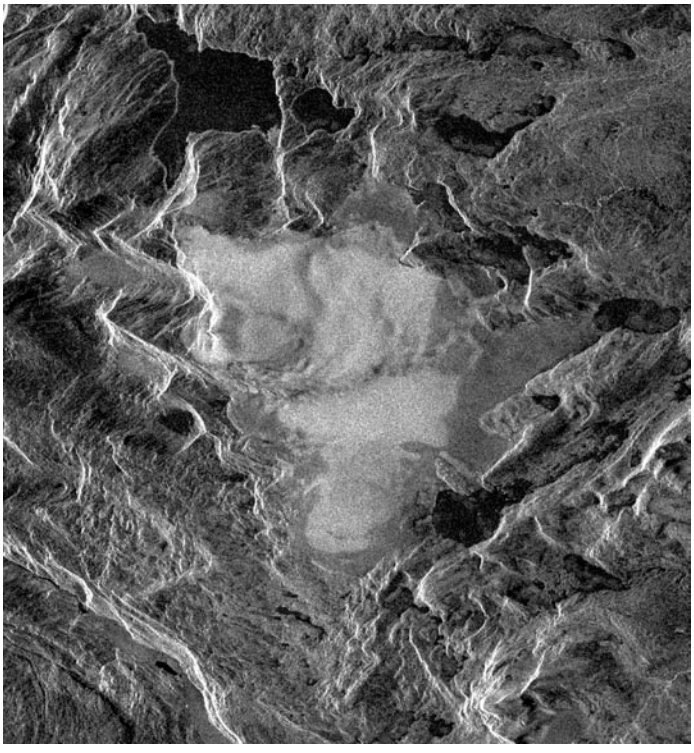

Figure 1. An example SAR image from February 19th 2000 (Image 2000-50). Note the backscatter contrast between the bright firn area and the darker bare ice zone.

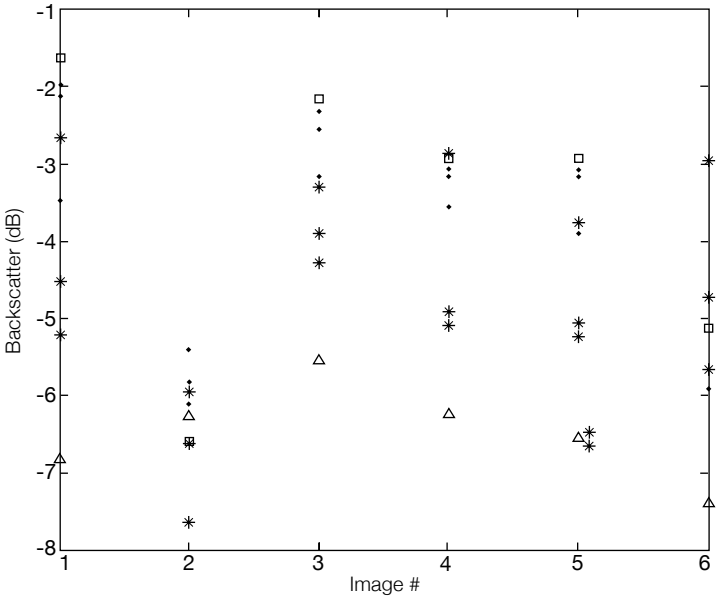

Figure 2. A graph showing the mean values of the different backscatter zones derived from digitized polygons. Samples represented by a diamond are from the firn area, those represented by an asterisk are areas of thin firn immediately above the firn limit. The triangles represent larger regions of melt identified in the ASTER image from 2001 and the squares represent melt regions in the ASTER data in the region of the GPR identified melt zones.

Continued from page 3

The larger melt patches and thin firn regions could be distinguished by their lower backscatter, although not in all images.

Our dataset comprises a range of beam types acquired during different seasons, testing the wider applicability of the method. The best performance was from the ST2 beam images acquired in late winter 2000 and the spring 2000 image. The image from November 2000 (2000-304) may have been influenced by recent melt-refreeze events producing anomalously bright signals from the region below the firn limit or a very rough surface causing greatly enhanced surface scattering than is normal. Radiometric correction of topographic effects would probably improve these results or at least dampen the effect of some of the anomalies. The georeferencing of the ASTER data should also be readdressed. Speckle filtering might also improve the signal analysis, but would result in smoothing, reducing the viability of small image samples.

These preliminary results suggest that scattering above the firn limit is strongly affected by the depth of firn and that melt effects might be detected in the firn area using SAR data. In all the images, the firn limit could be clearly delineated, but it is probable that this boundary equates to at least one meter of firn rather than the lowest limit of firn. A Rayleigh volume scattering model coupled with a surface scatter Small Peturbation Model estimated one meter of firn to have a backscatter of -6.78 dB (using in-situ measurements near the SAR firn limit). Below the "SAR firn limit" a polygon of 109 pixels averaged -7.09 dB in the images (range -6.57 dB to -8.74 dB) suggesting that the firn limit is better regarded as the firn gradient.

Submissions and Subscriptions

This newsletter, published by the Alaska Satellite Facility, was created to provide detailed information about special projects and noteworthy developments, as well as science articles highlighting the use of ASF data.

To receive the newsletter by postal mail, please fill out the subscription form linked to the ASF home page at www.asf.alaska.edu. Current and back issues of the newsletter can also be obtained in PDF format through the ASF web site.

Submissions to the *ASF News & Notes,* and suggestions about content are always welcome. If you are interested in contributing materials, please call or send an email to the editor:

Vicky Wolf, ASF User Services
907-474-6166 | uso@asf.alaska.edu

Alaska Satellite Facility
UAF Geophysical Institute
903 Koyukuk Drive
PO Box 757320
Fairbanks, AK 99775-7320